Estimation of Degradation Velocity of Biocompatible Damaged Stents due to Blood Flow

J. Dueñas-Pamplona, J. García, F. Castro, J. Muñoz-Paniagua and J. Sierra-Pallares

Estimation of degradation velocity of biocompatible damaged stents due to blood flow

Jorge Dueñas-Pamplona , Javier García , Francisco Castro , Jorge Muñoz-Paniagua , and José Sierra-Pallares

Abstract

Objective: Bioresorbable materials represent a promising technology for the treatment of coronary dis- ease. Among the different materials employed, magnesium stents display favourable mechanical properties. One of the main uncertainties regarding use is their behaviour when deployed on coronary bifurcations, especially when their retardant coating has been damaged during the implanta- tion process. This paper analyses the temporal evolution of the degradation of a damaged magnesium stent inserted into a coronary bifurcation. Methods: The rate of erosion- corrosion and the effect of the flow configuration on the mass transfer coefficient were estimated on the basis of previous experimental studies and numerical simulations. This coefficient has been employed to reproduce the con- ditions that can appear in real stent configurations, and computational fluid dynamics simulations were performed. Results: The diffusion coefficient for this particular case has been calculated from the mass transfer coefficient and the Sherwood number. The results of the simulation show how the presence of the inner artery wall has a positive effect, preventing a premature degradation of the stent, and how the distal strut is protected by the presence of the proximal struts. Conclusions: This study demonstrates the usefulness of the proposed methodology to evaluate the temporal evolution of the degradation of struts made of magnesium alloys. In addition, this methodology can be applied to a study of different materials and geometric configurations. Significance: The proposed technique can contribute to expanding existing knowledge concerning bioresorbable stent flow-corrosion, thus improving their design and implantation.

Index Terms

Biocompatible stents, computational fluid dynamics, coronary bifurcations, magnesium alloys.

Jorge Dueñas-Pamplona is with the Departamento de Ingeniería Energética, Escuela Técnica Superior de Ingenieros Industriales, Universidad Politécnica de Madrid, Madrid, Spain (e-mail: jorge.duenas.pamplona@upm.es).

Javier García and Jorge Muñoz-Paniagua are with the Departamento de Ingeniería Energética, Escuela Técnica Superior de Ingenieros Industriales, Universidad Politécnica de Madrid, Spain.

Francisco Castro and José Sierra-Pallares are with ITAP, and Departamento de Ingeniería Energética y Fluidomecánica, Escuela de Ingenierías Industriales, Universidad de Valladolid, Spain.

Digital Object Identifier 10.1109/TBME.2021.3076242

Introduction

The use of stents in cardiovascular diseases is very frequent. However, once the stent has fulfilled its objective, it becomes a problem, since it can be the origin of subacute thrombo- sis and in-stent restenosis. Therefore, the use of Biodegradable Stent / Scaffold (BDS) is now considered the fourth major evolution in Percutaneous Coronary Intervention (PCI) [1], since these stents have many of the characteristics of what could be considered the ideal. Such a stent would have to maintain its mechanical properties and then begin its degradation in the first three months following implantation, which entails a progressive loss of its mechanical properties. Finally, the stent would degrade completely without leaving remnants of its presence. This would allow restoration of the vessel contractile function and the possibility of re-implanting the stent in the same location in future interventions. In addition, the disappearance of the stent would allow the use of non-invasive diagnostic techniques such as Magnetic Resonance Imaging (MRI) and Computational Tomography(CT)[2].

There are two types of BDS: polymers and magnesium alloys. Polymer-based stents have much thicker struts than metallic ones due to their lower mechanical resistance, and need a heat supply for them to expand, which poses a risk to the artery wall. It is common to use magnesium alloys to build medical grafts such as orthopedic prostheses and stents because in biological fluids magnesium easily corrodes [1]. In addition, corrosion products can be absorbed or expelled by the human body and do not pose a problem. The biocompatibility of magnesium is very high, as it forms part of numerous biological mechanisms.

Several studies have addressed the behaviour of biocompatible stents in in vivo and in vitro scenarios. Regarding the degradation of stent materials in animal models, Zhang *et al.* [3] focused on the degradation and transport mechanism of an Mg-Nd-Zn-Zr stent in the carotid artery of rabbits over a period of 20 months, discovering that stent struts were mostly replaced in situ by degradation products after 4 months. The important finding was that the volume and calcium concentration of the degradation products decreased in the long term, dispelling clinicians' concerns regarding possible vessel calcification. Yang *et al.* [4] performed a similar investigation once again in rabbits, using a pure zinc stent located in the aorta. This stent was able to maintain mechanical integrity for 6 months and degraded by

41.75 ± 29.72 % of stent volume after 12-month implantation. In humans, it is worth noting the network meta-analysis of Kang *et al.* [5], which conducted a systematic review of 147 trials, showing the temporary drug eluting stents and Bioresorbable Stent / Scaffold (BRS) display a low risk of stent thrombosis after one year. This information, although useful, throws little light on the behaviour of stent material corrosion at the artery level; this is of paramount importance if there is to be an advance in this technology. Due to the limitations of the experiments, modelling represents a natural option for studying the behaviour of biocompatible stents at artery level. Several studies deal with the problem by using this approach. The literature shows that one of the major challenges is the intense chemical reactivity of magnesium [6]. The surface oxide film is very unstable and does not imply any protection. Its corrosion process is complex and significantly depends on the compositions of the alloy and that of the ambient fluid. Boland *et al.* [7] reviewed the computational modelling techniques used to describe the degradation of BRS. They describe different types of models: phenomenological or physical, with uniform, pitting or stress corrosion. Most of these models need to be calibrated. When analyzing the corrosion behaviour of an Magnesium Alloy Stent (MAS) the model must be applied to complex geometries, and multidimensional models should be considered [8]–[10]. Also, most of the studies deal with the problem of degradation exclusively in solids, but much less is known about corrosion behaviour in blood flow.

Chen *et al.* showed that the corrosion process is different if the ambient fluid is at rest or in motion [11]. The effect of the surrounding flow pattern on corrosion is very complex. In fact, it has been proven that the type of corrosion, its rate, morphologies and product formation are the function of Flow Induced Shear Stress (FISS) [12]. For example, high local FISS values can cause the release of corrosion products of a certain size that could result in stent facture and, as they move through the bloodstream, represent a real hazard. In addition, the influence of the flow changes with the evolution of the process. For example, according to [13] the shear stress on the wall has no initial effect, but its influence increases as the corrosion process persits. Therefore, it is important to analyze the effects of the local flow pattern on the degradation of struts made of magnesium alloy [12], [14].

The main problem of the MAS is the rapid corrosion involved [15], [16], as it does not allow its supporting effect to be sufficiently maintained until the artery heals. [17] developed a procedure to optimize the geometric design of a MAS in order to increase its corrosion resistance. In other cases, a coating has been chosen to delay the corrosion process. Biodegradable polyester or magnesium fluoride coatings are used to control its degradation rate. However, a frequent problem is that, during the implantation of the stents, fissures appear on the coating due to the rubbing of the stent against the calcium deposits in the capillary vessels on the way to the implantation point [18]. Thus, there may be areas of the stent where corrosion is more rapid than in others, due to the damage of the retardant coating. This problem is especially important if the stent is to be implanted in coronary bifurcations. Premature erosion-corrosion could lead to embolization of the stent, causing even more damage.

In spite of the medical relevance of the problem, relatively little research has been reported on the temporal degradation of biocompatible stents at artery level, information which is critically important when using a Bioresorbable Stent / Scaffold (BRS) in coronary bifurcations. Thus, the objective of this paper is to analyze, by means of Computational Fluid Dynamics (CFD), the time taken for a BRS to degrade when its retardant coating has been damaged during implantation processes under the action of blood flow.

The influence of the location of the fissure on this evolution will be analyzed. For this purpose, it is necessary first of all to determine the rate of erosion-corrosion of the stent in blood, and the effect of the flow configuration on mass transfer.

METHODS

Erosion-Corrosion Model

The purpose of this section is to explore the relationship between blood flow and BRS degradation. Magnesium erosion-corrosion in blood encompasses a wide range of flow induced corrosion processes. Due to the joint action of mechanical forces and chemical species in dissolution, the blood-accelerated corrosion may be accompanied by erosion of the underlying metal. This joint action of erosion and corrosion is known as erosion-corrosion [19]. The corrosion reaction taking place is [6]:

$$\mathrm{Mg} \longrightarrow \mathrm{Mg^{2+}} + 2\mathrm{e^-}, \tag{1}$$

$$2\mathrm{H_2O} + 2\mathrm{e^-} \longrightarrow \mathrm{H_2} + 2\mathrm{OH^-}, \tag{2}$$

$$2\mathrm{H_2O} + \mathrm{O_2} + 4\mathrm{e^-} \longrightarrow 4\mathrm{OH^-}, \tag{3}$$

$$\mathrm{Mg^{2+}} + 2\mathrm{OH^-} + \longrightarrow \mathrm{Mg(OH)_2}. \tag{4}$$

Some authors [15], [20] also report the important influence of Cl^- ion in the corrosion process, via its effect on $\mathrm{Mg(OH)_2}$:

$$\mathrm{Mg(OH)_2} + 2\mathrm{Cl^-} \longrightarrow \mathrm{MgCl_2} + 2\mathrm{OH^-}. \tag{5}$$

Pitting is produced due to the effect of $\mathrm{Cl^-}$ and eroded magnesium metal may disintegrate from the whole strut as irregular particles and fall into the surrounding media. Blood flow may produce fluid shear stress and influence the deposition of a corrosion product layer or, on the other hand, take away the locally generated $\mathrm{OH^-}$ ions, thus affecting corrosion behavior [14].

Some authors propose the erosion–corrosion process can be assumed to be under the control of oxygen mass-transfer to the corroding surface [21]. Thus, the erosion-corrosion rate can be calculated by applying well-established mass transfer correlations of dimensionless groups:

$$\mathrm{Sh} = \mathrm{Sh_0} + \mathsf{C}_1 \mathrm{Re}^{a_1} \mathrm{Sc}^{\beta}, \tag{6}$$

where Sh is the Sherwood number, $\mathrm{Sh_0}$ is the Sherwood number under no flow conditions, Re is the Reynolds number, Sc is the Schmidt number and C_1, a_1 and β are constants. This equation results from the non-dimensional form of the steady flow equations for incompressible fluids, where mass forces are not relevant [22],

$$\hat{\nabla} \cdot \hat{\underline{v}} = 0 \tag{7}$$

$$\frac{D\hat{\underline{v}}}{D\hat{t}} = \frac{1}{\mathrm{Re}}\hat{\nabla}^2\hat{\underline{v}} - \hat{\nabla}\hat{\mathrm{P}} \tag{8}$$

$$\frac{D\hat{Y}_a}{D\hat{t}} = \frac{1}{\mathrm{Re\,Sc}}\hat{\nabla}^2\hat{Y}_a \tag{9}$$

where $\hat{\underline{v}}$ is the non-dimensional velocity, $\hat{\mathrm{P}}$ is the non-dimensional reduced pressure and $\hat{Y}_a$ is the non-dimensional mass fraction of component a. The Sherwood number appears here after an analysis of the boundary conditions and is defined as

$$\mathrm{Sh} = \frac{h_m L}{\Gamma}, \tag{10}$$

where h_m is a global mass transfer coefficient obtained by analogy to the heat transfer coefficient, Γ is the local diffusion coefficient and L is a characteristic length. h_m and Γ have the relation:

$$h_m = \frac{1}{A(Y_s - Y_\infty)} \int_A (\Gamma \nabla Y) \cdot \underline{n}\, dA, \tag{11}$$

where the integral is evaluated at the corroding surface, Y_s is the mass fraction of magnesium on the corroding surface and Y_∞ is the mass fraction of magnesium at a distance from it.

If the velocity and mass fraction fields together with the Γ coefficient are available for a particular flow configuration, it is possible to estimate the erosion-corrosion velocity for a magnesium stent by means of calculating the Sherwood number and h_m. This approach, although simple, has proven to be effective when estimating erosion-corrosion of engineering materials in contact with liquids [12], [23], since it is possible to compute the mass fraction and velocity fields by means of a CFD code.

To use this methodology for blood-triggered corrosion it is necessary to estimate the value of Γ for a particular alloy in blood-flow conditions. Thus, the use of experimental data is required to fit a correlation like the one given by (6). In the literature several experiments can be found relating to magnesium erosion-corrosion using blood and Simulated Body Fluids (SBF) in dynamic conditions. One of the most interesting results has been obtained by Geis-Gertorfer *et al.* [24], who analyze magnesium stent degradation during six hours of immersion in blood using a Chandler-Loop model with different magnesium alloys. The Chandler - Loop system employed in this research attempts to mimic blood flow over a magnesium probe in a real artery by means of a closed toroidal loop rotating in an isothermal bath at constant velocity. This movement creates a relative motion of the fluid similar to a laminar flow profile, resembling a physiological scenario. Geis-Gesterfer *et al.* experimented with different probes and determined the mass loss of each probe gravimetrically. This configuration, however, creates a problem: as erosion-corrosion develops on the magnesium probe, ions are continually accumulating in the blood sample. Therefore, the mass fraction of Cl^- is continuously growing because washing does not take place, resulting in an environment which does not resemble what is happening in a real artery, where Cl^- ions would be continuosuly washed by the main blood flow.

To overcome this drawback, information based on experimentation with SBF might be used. Very often, these experiments are carried out in a flow rig with a much greater amount of fluid. The flow continuously washes the corroding surface [14] and dilutes the concentration of ions. In this paper, estimation of the erosion-corrosion rate is based on the experimental data obtained by Soya *et al.* [13] using SBFs. They describe the effect of the fluid flow rate, surface roughness and strain level on the corrosion behavior of magnesium alloy AZ31 probes, characterized in a custom test bench where a continuous flow is achieved. This research is attractive because the experiments are easily reproducible in a CFD simulation. Figure 1 outlines the flow configuration and main dimensions of the magnesium probes and the main pipe.

The mass loss per surface area of every magnesium probe was obtained over time (Fig. 3). This loss is related to the global mass transfer coefficient h_m in a control volume like that of Figure 1:

$$\frac{\text{mass loss}}{\text{surface area}} = h_m\,(Y_{Mg,s} - Y_{Mg,\infty})\,t \tag{12}$$

where $Y_{Mg,s}$ and $Y_{Mg,\infty}$ are the mass fractions of magnesium on the probe surface and in the bulk flow of the control volume and t is the time. $Y_{Mg,s} \approx 1$ and $Y_{Mg,\infty} \approx 0$ due to the high degree of dilution. Figure 2 shows the points where the driving force is established. Although different choices can be made for the driving force – the magnesium species will be more concentrated in the wake, for instance – magnesium will be always highly diluted. Thus,

$$\frac{\text{mass loss}}{\text{surface area}} \approx h_m t \tag{13}$$

and h_m can be estimated from a linear fitting to the data presented in Figure 3. It is worth noting here that this value is constant for the experimental data of [13], but this is only valid as long as the material loss is negligible in comparison with the total probe mass. If the geometry changes over time due to the action of corrosion, h_m would be altered because of the flow around the probe and therefore the species gradient would also change.

Mass Transfer Correlation Determination

Determining the local mass transfer diffusion coefficient Γ that fits the mass transfer coefficient h_m obtained experimentally is not a straightforward process. There is no easy way to estimate Γ, and it is neccesary to obtain the mass fraction gradient ∇Y for the magnesium species using the real geometry in order to fit it. To this end, Soya's geometry is meshed and analysed using CFD with the commercial software `ANSYS Fluent 19.2`. Simulation is carried out by means of a coupled solver on the assumption that a laminar flow is present due to the low value of the Reynolds number in the experiments ($\mathrm{O}(\mathrm{Re}) \approx 10^2$). Third-order discretizacion schemes are used for all variables. The mass fraction field is determined by the equation

$$\rho\frac{DY_{Mg}}{Dt} = \Gamma\nabla^2 Y_{Mg} \tag{14}$$

and boundary conditions are fixed as follows: $Y_{Mg} = 0$ at the inlets (a thorough washing is considered due to dilution in the

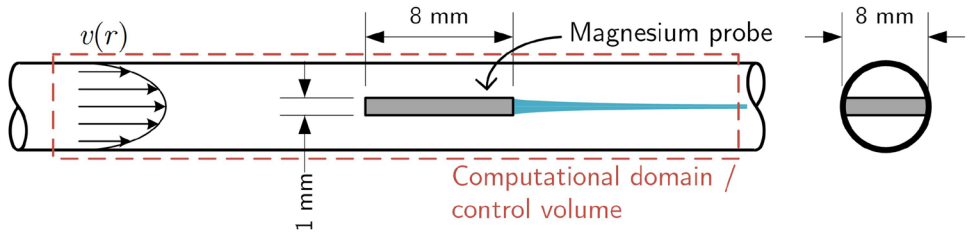

Fig. 1. Sketch of the computational model employed to simulate Soya *et al.* [13] experimental set-up.

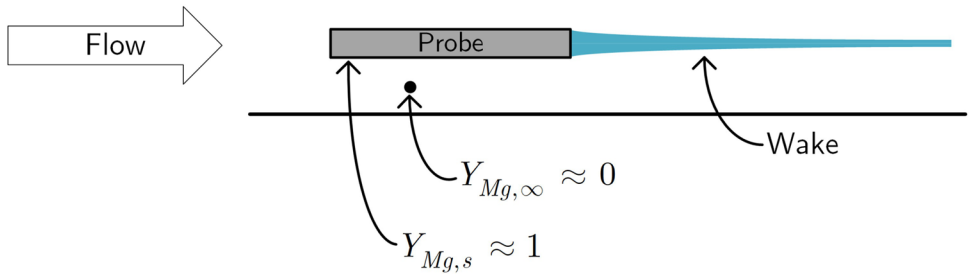

Fig. 2. Driving force definition.

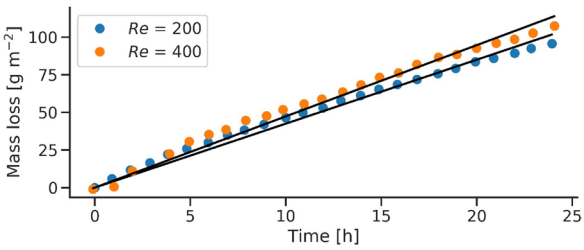

Fig. 3. Soya *et al.* [13] experimental data for two Reynolds numbers.

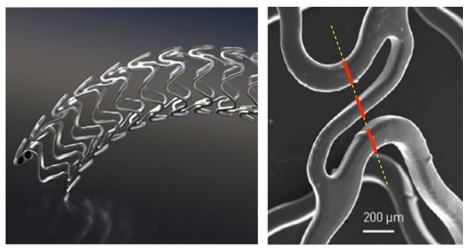

Fig. 4. Stent geometry. (a) Whole stent, (b) Connector regions. The discontinous line marks, in red, the proximal, medial and distal sections, which have been used to perform simulations 2, 3, and 4.

flow rig), $Y_{Mg} = 1$ at the corroding surface (see Fig. 2) and $\partial Y_{Mg}/\partial n = 0$ at the other surfaces.

Since a correlation similar to (6) is to be determined, a Design Of Experiments (DOE) using Latin Hypercube Sampling is performed. Input variables are average inlet velocity and the mass transfer coefficient Γ. The following intervals have been used:

$$\begin{cases} \bar{v} \in [0.02,\ 0.3]\ ms^{-1} \\ \Gamma \in \left[10^{-9},\ 10^{-6}\right]\ kgm^{-1}s^{-1}, \end{cases} \tag{15}$$

which corresponds to non dimensional numbers in the range:

$$\begin{cases} \mathrm{Re} \in [50,\ 720] \\ \mathrm{Sc} \in \left[10^{3},\ 10^{6}\right]. \end{cases} \tag{16}$$

These values match the Reynolds number values reported by Soya as well as a sufficiently wide range of Schmidt numbers according to similar studies found in the literature [25]. The output variables are mass flux at the surface of the corroding probe, $G_{Mg} = \int_A \Gamma \nabla Y \cdot \_n\, dA$ and the average Wall Shear Stress (WSS) on the magnesium probe. Fifty numerical experiments are performed. In this way, it is possible to generate enough data to determine a correlation similar to (6) for Soya's experiment. By using this correlation along with experimental data of mass loss supplied in [13], it is possible to estimate Γ with the experimentally available h_m.

Numerical Model

In this paper a simplified geometry is contemplated for a bioresorbable magnesium stent (4 a) as a means of assessing the proposed degradation model. An axisymmetric configuration has been chosen to perform the numerical simulations, in which three struts, namely, proximal, medial and distal, have been considered. No more rings are included in the calculation because, as the distance between the struts is sufficiently large, the flow reattaches before reaching the next strut. This results in the same incoming flow regardless of the number of struts located upstream.

In view of the stent structure and the possible flow scenarios, a range of different cases have been calculated. First, we have

TABLE I
SUMMARY OF THE CONFIGURATIONS CONTEMPLATED

Letter: indicating the stent position relative to the artery wall	
a: Well-apposed stents	Struts in contact with the artery wall
b: Malapposed stents	Struts at a distance from the artery wall
Number: indicating the strut undergoing degradation	
1: Outer layer strut	Struts separated by distance between rings
2: Proximal strut	Connector regions, struts separated by width of struts
3: Distal strut	Connector regions, struts separated by width of struts
4: Medial strut	Connector regions, struts separated by width of struts

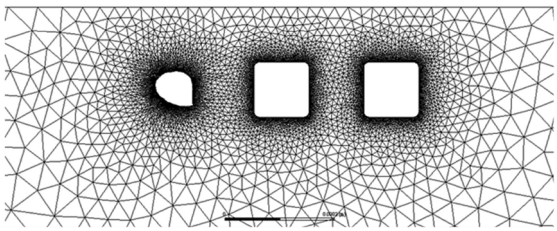

Fig. 5. Intermediate stage of the dynamic mesh during the calculation process, which, in this case, represents degradation of the proximal strut in the connector regions of a malapposed stent.

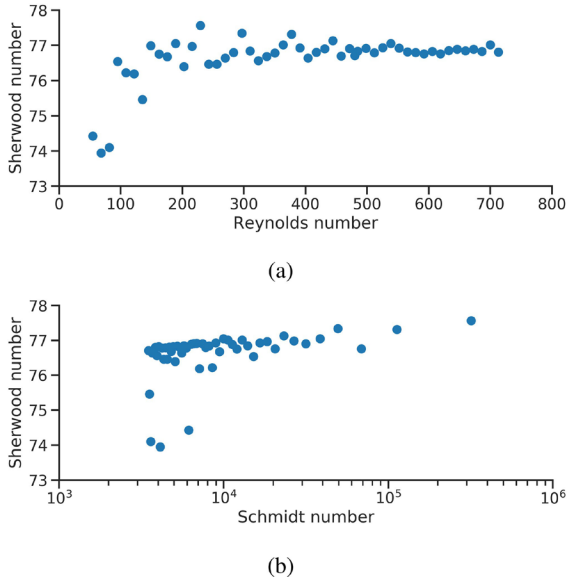

Fig. 6. Sherwood number dependency Vs. (a) Reynolds number, (b) Schmidt number.

differentiated between well apposed (cases a) or malapposed stents (cases b). For the former, the struts are in close contact with the artery wall, while for the latter there is a distance between the struts and the artery wall, which we have supposed to be equal to the height of the strut. Furthermore, for each case four different setups have been considered, depending on which strut displays the microcrack that will lead to an early degradation process. The first set-up considers the damage to the outer polymeric layer of a ring strut, while in the next three set-ups the microcrack is assumed to be in the proximal, medial or distal struts of the connector regions (4 b). The width and height strut were 150μm, and the diameter of the idealized artery was 3mm. A summary of all the different cases can be found in Table I.

A triangular mesh is used, which is refined near the stent struts to capture the corresponding geometry. The mesh has between 30 000 and 35 000 cells depending on the case. The dynamic mesh capability of the commercial code `ANSYS Fluent 19.2` is implemented. This meshing technique allows a moving and deforming mesh capable of simulating the degradation process; an intermediate stage of the dynamic mesh during the calculation process is shown in Figure 5. The strut boundary is moved according to the gradient value of the passive scalar close to the strut wall, decreasing the surface area in the same way as the magnesium reduction predicted by the model. The arterial wall is considered to be rigid. This is a reasonable assumption for regions where a percutaneous intervention is performed, as both the formation of atheromatous plaques and the presence of the stent contribute to a reduction in vessel elasticity. The fluid is assumed to be Newtonian, with a viscosity $\mu = 0.0035$ kgm^{-1}.s^{-1} and density $\rho = 1050$ kgm^{-3} [26], (the Reynolds number is equal to 180). In addition to the mass and momentum equations, a scalar transport equation is resolved, as it is required to implement the corrosion model.

Due to the large difference between the time scales for diffusion and coronary pulsatile flow, a steady boundary condition for the inlet flow is assumed. At the inlet, a constant velocity equal to 0.2 ms^{-1} is imposed [27], while at the outlet an outflow boundary condition is specified to preserve mass conservation. A time step equal to 0.001s was used to ensure a Courant Friedichs Levy condition (CFL) below 1. The degradation model inferred from Soya's experiments was adjusted by dynamic similarity so as to simulate complete stent degradation, with a computational time step of 0.001 equivalent to a real time of 1s. We have assumed that the different time scales associated to the diffusion and convection processes allow us to scale the degradation constant and speed up simulation.

RESULTS

Mass Transfer Coefficient Estimation

Numerical experiments according to the DOE explained in Section 2.1 were run and analyzed. As a result of these, Reynolds, Schmidt and Sherwood numbers, along with WSS, were obtained. The Sherwood number is calculated by using its definition (10). Figure 6 shows the dependency of Sherwood numbers with respect to Reynolds and Schmidt numbers. The results show how the Sherwood number remains almost constant for the design space studied here, oscillating between 74 and 77, whilst Reynolds and Schmidt numbers are low.

It is possible to obtain an alternative expression for the Sherwood number by introducing $\mathrm{Re} = KC_f^{a_2}$ in Eq. (6):

$$\mathrm{Sh} = \mathrm{Sh}_0 + C_1 \quad KC_f^{a_2} \quad \mathrm{Sc}^{\beta}, \tag{17}$$

thus

$$\mathrm{Sh} = \mathrm{Sh}_0 + C_2 C_f^{a_2} \mathrm{Sc}^{\beta}, \tag{18}$$

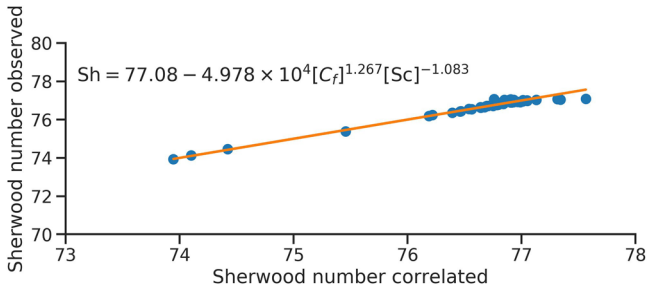

Fig. 7. Sherwood correlation in terms of C_f and Schmidt number.

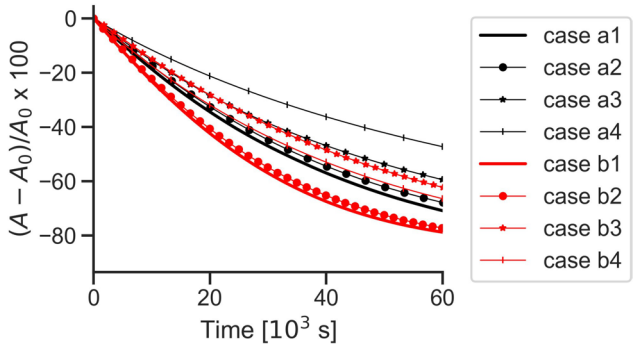

Fig. 8. Transient evolution of mass loss.

where

$$C_2 = KC_1, \tag{19}$$

since K is a constant. By applying the above 18, it is possible to describe the erosion-corrosion process in terms of WSS and the Schmidt number. This seems to be more appropriate according to the literature [19]. In order to fit Sh_0, C_2, a_2 and β in (18) a least-quares algorithm is used. This relation is shown in Figure 7. The equation

$$Sh = 77.08 - 4.798 \times 10^4 \, (C_f)^{1.267} \, (Sc)^{-1.083} \tag{20}$$

represents a very good approximation ($R^2 \approx 0.97$) of the numerical data under analysis.

It is worth noting here that the Sherwood number remains more or less constant, in the range of the Schmidt and Reynolds number we are studying. That is, the degradation rate is constant in spite of the change in the Reynolds number and, thus, in WSS over the probe. This result is not surprising. Indeed, if we pay attention to similar numerical experiments described in the literature, constant Sherwood numbers are also found in the laminar flow through tubes and slits when the driving force is constant [22]. In those situations, the mass transfer coefficient h_m remains constant, and, consequently, the Sherwood number also. This is due to the very low mass transfer from the probe to the bulk fluid, which makes it almost impossible to significantly disrupt bulk concentration. Thus, the Sherwood number can be approximated by

$$Sh \approx Sh_0 = 77.08 \tag{21}$$

TABLE II
MASS TRANSFER COEFFICIENTS ESTIMATED FROM [13]

Experiment	Re	h_m/kg m^{-2} s^{-1}
1	200	1.179×10^{-6}
2	400	1.314×10^{-6}

Although this value was obtained for a range of diffusion coefficients, see Eq. (15), it is extendible to lower values of Γ due to its asymptotic nature.

According to Soya's experiments, the mass loss of the magnesium probe over time is almost linear (Fig. 3). The global mass transfer estimated from Soya's experiments are presented in Table II.

The mass transfer coefficient h_m changes slightly, that is, around 11%, when the Reynolds number is doubled. Although the change is not a substantial one, it is significant. This suggests that the hypothesis of oxygen mass transfer as a controlling step of the erosion-corrosion process is not entirely accurate, and it can only be understood as an approximation. With the data provided in Table II and the asymptotic Sherwood number, Eq. (21), it is possible to calculate a mean diffusion coefficient for the erosion-corrosion process in the experiment conducted by Soya:

$$\Gamma = \frac{\bar{h}_m D}{Sh} = 1.294 \times 10^{-10} kgm^{-1}s^{-1}, \tag{22}$$

where $\bar{h}_m$ is the average of experimental mass transfer coefficients shown in Table II and D is the pipe diameter. This coefficient is practically independent of the Reynolds number, and capable of being used in CFD computations of mass transfer.

Simplified Stented Artery

The aim is to study cases where one of the struts is damaged due to the implantation procedure. In these situations, the magnesium core is exposed to blood flow and the strut degrades faster, affecting the mechanical properties of the stent and decreasing its safety and reliability. It is assumed that in each configuration only one strut is damaged and its corresponding coating completely removed. We have also hypothesize that the degradation process of the damaged strut occurs during a shorter period than that of revascularization time, so the stent is in contact with the flow during the whole of the simulation process and the inner artery wall remains in the same place. It should be mentioned that only aspects of fluid mechanics will now be considered.

As seen in the previous section regarding the numerical model, the proposed model is applied to an axisymmetric configuration, with struts of the typical dimensions in MAS. Different cases have been considered, with an effort being made to reproduce as far as possible the conditions that may appear in real stent implantations (Table I). A first group (cases a) corresponds to the correct deployment of the stent inside the artery, the struts being, therefore, in contact with the inner wall (Figure 9). The second group (cases b) refers to malapposed stents, where the

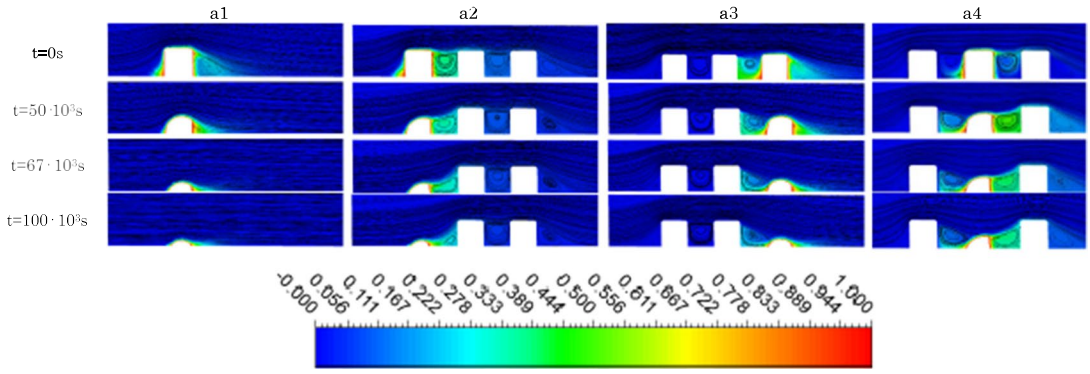

Fig. 9. Temporal strut evolution for case a (well-apposed stent). The color map corresponds to the magnesium mass fraction.

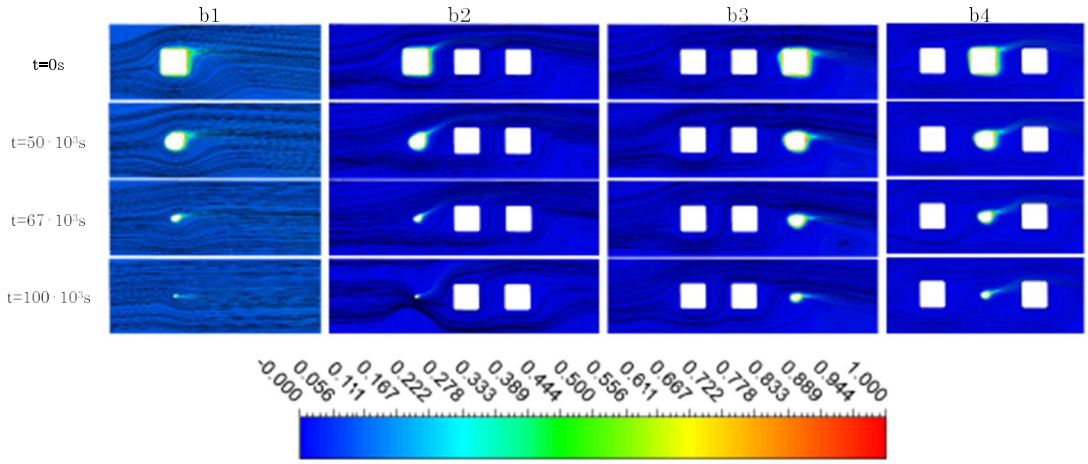

Fig. 10. Temporal strut evolution for case b (malapposed stent). The color map corresponds to the magnesium mass fraction.

distance between the struts and the inner wall is equal to the height of the strut (Figure 10).

For each group, four different set-ups are taken into account. The first corresponds to three struts separated at a distance equal to the space between the rings (see Figure 4 a), and only the proximal strut is supposed to be damaged and affected by degradation (in the figures only the proximal strut is represented). Calculations have also been made in terms of the degradation of the distal strut; yet here the results obtained are the same as for the proximal strut, as the distance between the struts is sufficiently large and the flow reattaches before the next strut, with the flow conditions consequently being the same for the proximal and distal strut. For this reason, only proximal strut cases are presented in this paper. In the second, third and fourth set-ups there is an attempt to reproduce the flow conditions around the connectors between the rings (see Figure 4 b). Three struts separated by a distance equal to the width of struts are considered. For each of the cases one of the struts is subject to degradation, due to the presence of a microcrack: the proximal, medial or distal, respectively.

As indicated in the previous section, mass loss displays locally an almost linear behaviour with respect to time, where the constant h_m is the mass transfer coefficient that depends on the diffusion coefficient Γ and the mass fraction gradient of magnesium ∇Y. In the simulations, the surface nodes have been moved to the interior to produce an equal amount of mass loss.

TABLE III
STENT DEGRADATION FOR $t = 60 \times 10^3 s$

Case	Degradation (%) $(A - A_0)/A_0 * 100$	((Degrad.-Degrad. a1)/Degrad. a1) *100
a1	−73.97	0
a2	−70.91	−4.14
a3	−62.64	−15.31
b1	−80.58	8.94
b2	−79.38	7.31
b3	−65.70	−11.18

The transient evolution for these eight cases is depicted in Figure 8. Black lines correspond to group a (well-apposed struts) and red lines to group b (malapposed struts). Degradation occurs more rapidly for group b. This can be explained by observing the concentration of magnesium around the struts (Figures 9 and 10), where re-circulation is greater for group a than for group b, with the consequent lower concentration gradient near the strut. The presence of the inner artery wall has a positive effect, preventing a premature degradation of the bioresorbable stent. This behavior is quantified in Table III for $t = 60 \times 10^3 s$.

Figures 9 and 10 visualize temporal strut evolution for both a well-apposed and malapposed stent, respectively. Both initial-stage cases (i.e. t = 0 s), in which no degradation has yet been observed, can be validated with studies run for wall-mounted cubes and isolated square-cylinders. For the latter, the authors are not aware of experimental or numerical data at Re = 180 considering single or tandem rounded 2-D square cylinders. However, the flow topology observed at Re = 100 for a 2-D square cylinder with sharp corners, where the flow is not detached from the upstream corners, is similar to that obtained for Re = 175 when rounded corners are considered, [28]. In fact, although the Reynolds number is greater for the latter, the corner roundness contributes towards additional shear stress, and thus flow follows the lateral contours instead of upstream corner separation, which is in agreement with our results, as is observed in Fig. 10 for the b1 case at t = 0 s. Cases b2 to b4 are similar from a flow topology approach at t = 0 s. The distance between two successive struts is $L = 2w$, where w is the width of the strut. In [29] it is observed that when $L/w = 2$, the flow becomes unsteady in the far wake, as is observed in Fig. 10. In [30], the flow along an inline sharp-corner square cylinder array being studied for different L/w values at Re = 100. When this is lower than 3.0, no vortex shedding occurs in the gap, as shown in Fig. 10.

If we compare cases 1, 2, 3 and 4 for both groups, strut degradation is more rapid for case 1, where the flow dispels the magnesium, decreasing the concentration gradient near the strut. Regarding cases 2, 3 and 4, mass loss is greater when the strut in question is in proximal position (case 2), and a recirculation bubble is observed essentially behind the strut. Case 3 corresponds to a distal strut degradation. In this case, the flow is disrupted by the presence of the proximal struts and the wake around the distal strut is slightly more intense, producing a small increase in magnesium near the strut and, therefore, less degradation. Case a4 is highly influenced by the presence of both the proximal and distal struts, intensifying local magnesium concentration and thus decreasing mass loss. However, in case b4 degradation is slightly more intense than in b3, which is due to the passing flow between the proximal and distal struts (higher than in a3, where the distal strut was in the wake of the previous strut). It should be noted that in these simulations the whole strut is exposed to the flow, assuming the corresponding coating has disappeared. This is a very unfavorable case, since in real implantations only microcracks are expected and the degradation process will be slower.

Conclusion

A new method has been proposed to analyze the effects of the local flow blood pattern on the development of the degradation of MAS. Due to the frequent appearance of microcracks on the retardant coating, a methodology is put forward to study degradation due to the erosion and corrosion induced by blood flow. The rate of erosion-corrosion and the effect of the flow configuration on the mass transfer coefficient were estimated using available experimental data. The effect of the surrounding flow pattern on the erosion-corrosion process is very complex: during the study of the relationship between blood flow and BRS degradation the global mass transfer coefficient h_m was considered constant, as long as the material loss was negligible in comparison with the total probe mass. The Reynolds, Schmidt and Sherwood numbers were obtained from a set of numerical experiments and the Sherwood number remained constant over the range of studies, thereby allowing a local diffusion coefficient Γ to be calculated. This value has been employed to reproduce as far as possible the conditions that can appear in real stent implantations, and different case studies were considered where the proximal or distal coating was damaged due to the implantation procedure. The results show that the presence of the inner artery wall has a positive effect, avoiding premature degradation of the stent. In terms of the medial and distal struts, the flow is disrupted by the presence of the proximal struts and, as expected, degradation decreases.

Limitations of this study include the simplified 2D geometry of the stent, and the fact that the whole strut is exposed to the flow, assuming that the corresponding coating has disappeared. In a future study, a more complex and realistic 3D model will be developed, including the effect of local microcracks and the retardant coating on the time development of overall degradation.

Acknowledgment

The authors would like to express their gratitude to the Programa Propio - Universidad Politécnica de Madrid, especially for its predoctoral contract grants. They would also like to thank the CeSViMa UPM project for its computational resources.

References

[1] T. Hu *et al.*, "Biodegradable stents for coronary artery disease treatment: recent advances and future perspectives," *Mater. Sci. Eng. C., Mater. Bio. Appl.*, vol. 91, pp. 163–178, Oct. 2018.

[2] C. Di Mario *et al.*, "Drug-eluting bioabsorbable magnesium stent," *J. Interventional Cardiol.*, vol. 17, no. 6, pp. 391–395, Dec. 2004.

[3] J. Zhang *et al.*, "The degradation and transport mechanism of a Mg-Nd-Zn-Zr stent in rabbit common carotid artery: A 20-month study," *Acta Biomaterialia*, vol. 69, pp. 372–384, Mar. 2018.

[4] H. Yang *et al.*, "Evolution of the degradation mechanism of pure zinc stent in the one-year study of rabbit abdominal aorta model," *Biomaterials*, vol. 145, pp. 92–105, Nov. 2017.

[5] S.-H. Kang *et al.*, "Stent thrombosis with drug-eluting stents and bioresorbable scaffolds: Evidence from a network meta-analysis of 147 trials," *JACC. Cardiovasc. Interventions*, vol. 9, no. 12, pp. 1203–1212, Jul. 2016.

[6] Y. F. Zheng, X. N. Gu, and F. Witte, "Biodegradable metals," *Mater. Sci. Eng. R: Rep.*, vol. 77, pp. 1–34, Mar. 2014.

[7] E. L. Boland *et al.*, "A review of material degradation modelling for the analysis and design of bioabsorbable stents," *Ann. Biomed. Eng.*, vol. 44, no. 2, pp. 341–356, Feb. 2016.

[8] Z. Shen *et al.*, "Predicting the degradation behavior of magnesium alloys with a diffusion-based theoretical model and in vitro corrosion testing," *J. Mater. Sci. Technol.*, vol. 35, no. 7, pp. 1393–1402, Jul. 2019.

[9] J. A. Grogan, S. B. Leen, and P. E. McHugh, "A physical corrosion model for bioabsorbable metal stents," *Acta Biomaterialia*, vol. 10, no. 5, pp. 2313–2322, May 2014.

[10] Y. Gao *et al.*, "A quantitative study on magnesium alloy stent biodegradation," *J. Biomech.*, vol. 74, pp. 98–105, Jun. 2018.

[11] Y. Chen *et al.*, "Dynamic degradation behavior of MgZn alloy in circulating m-SBF," *Mater. Lett.*, vol. 64, no. 18, pp. 1996–1999, Sep. 2010.

[12] J. Wang *et al.*, "Flow-induced corrosion of absorbable magnesium alloy: In-situ and real-time electrochemical study," *Corrosion Sci.*, vol. 104, pp. 277–289, Mar. 2016.

[13] Y. Soya *et al.*, "Corrosion behavior of engineering materials in flow field," *Adv. Mater. Res.*, vol. 922, pp. 722–727, 2014, doi: 10.4028/www.scientific.net/amr.922.722.
[14] J. Lévesque *et al.*, "Design of a pseudo-physiological test bench specific to the development of biodegradable metallic biomaterials," *Acta Biomaterialia*, vol. 4, no. 2, pp. 284–295, Mar. 2008.
[15] D. Liu *et al.*, "Degradation mechanism of magnesium alloy stent under simulated human micro-stress environment," *Mater. Sci. Eng. C., Mater. Biol. Appl.*, vol. 84, pp. 263–270, Mar. 2018.
[16] W. Wu *et al.*, "Experimental data confirm numerical modeling of the degradation process of magnesium alloys stents," *Acta Biomaterialia*, vol. 9, no. 10, pp. 8730–8739, Nov. 2013.
[17] W. Wu *et al.*, "Finite element shape optimization for biodegradable magnesium alloy stents," *Ann. Biomed. Eng.*, vol. 38, no. 9, pp. 2829–2840, Sep. 2010.
[18] T. Y. Qiu, L. G. Zhao, and M. Song, "A computational study of mechanical performance of bioresorbable polymeric stents with design variations," *Cardiovasc. Eng. Technol.*, vol. 10, no. 1, pp. 46–60, Mar. 2019.
[19] R. W. Revie and H. H. Uhlig, *Uhlig's corrosion handbook*, 3rd ed., ser. *Electrochem. Soc. Ser.*. Hoboken N.J.: Wiley, Apr. 2011.
[20] J. Wang *et al.*, "Microstructure and corrosion properties of as sub-rapid solidification Mg-Zn-Y-Nd alloy in dynamic simulated body fluid for vascular stent application," *J. Mater. Sci. Mater. Med.*, vol. 21, no. 7, pp. 2001-2008, Jul. 2010.
[21] C. Davis and P. Frawley, "Modelling of erosion-corrosion in practical geometries," *Corrosion Sci.*, vol. 51, no. 4, pp. 769–775, Apr. 2009.
[22] R. B. Bird, W. E. Stewart, and E. N. Lightfoot, *Transport Phenomena*, *2nd ed*. New York: Wiley, 2007.
[23] L. Jingjun, L. Yuzhen, and L. Xiaoyu, "Numerical simulation for carbon steel flow-induced corrosion in high-velocity flow seawater," *Anti-Corrosion Methods Mater.*, vol. 55, no. 2, pp. 66–72, Mar. 2008.
[24] J. Geis-Gerstorfer *et al.*, "Blood triggered corrosion of magnesium alloys," *Mater. Sci. Eng. B*, vol. 176, no. 20, pp. 1761–1766, Dec. 2011.
[25] P. R. S. Vijayaratnam, J. A. Reizes, and T. J. Barber, "Flow-mediated drug transport from drug-eluting stents is negligible: Numerical and in-vitro investigations," *Ann. Biomed. Eng.*, vol. 47, no. 3, pp. 878–890, Mar. 2019.
[26] A. O. Frank, P. W. Walsh, and J. E. Moore Jr, "Computational fluid dynamics and stent design," *Artif. Organs*, vol. 26, no. 7, pp. 614–621, Jul. 2002.
[27] J. G. García *et al.*, "Effects of bifurcation-specific and conventional stents on coronary bifurcation flow. An experimental and numerical study," *J. Biomech.*, vol. 54, pp. 64–72, Mar. 2017.
[28] T. Ambreen and M.-H. Kim, "Flow and heat transfer characteristics over a square cylinder with corner modifications," *Int. J. Heat Mass Transfer*, vol. 117, pp. 50–57, Feb. 2018.
[29] A. Lankadasu and S. Vengadesan, "Interference effect of two equal-sized square cylinders in tandem arrangement: With planar shear flow," *Int. J. Numer. Methods Fluids*, vol. 57, no. 8, pp. 1005–1021, Jul. 2008.
[30] Y. Bao, Q. Wu, and D. Zhou, "Numerical investigation of flow around an inline square cylinder array with different spacing ratios," *Comput. Fluids*, vol. 55, pp. 118–131, Feb. 2012.